Numerical investigation on the performance enhancement of PEMFC with gradient sinusoidal-wave fins in cathode channel

Zhijie Chen[a] Wei Zuo[a, d*] Kun Zhou[a,d] Qingqing Li[a, d] Zhengming Yi[a, d] Yuhan Huang[b, c]

a. The State Key Laboratory of Refractories and Metallurgy, Wuhan University of Science and Technology, Wuhan 430081, China

b. Centre for Green Technology, School of Civil and Environmental Engineering, University of Technology Sydney, NSW 2007, Australia

c. Department of Engineering Science, University of Oxford, Oxford OX1 3PJ, United Kingdom

d. National-provincial Joint Engineering Research Center of High Temperature Materials and Lining Technology, Wuhan University of Science and Technology, Wuhan 430081, China

**zuowei@wust.edu.cn*

Abstract: As the cathode channel structure plays significant effects on the performance of the proton exchange membrane fuel cell (PEMFC), in this work, a 3D multi-phase model of PEMFC is established and effects of cathode channel structure (conventional channel, normal sinusoidal-wave fins and gradient sinusoidal-wave fins) on the performance of PEMFC are numerically investigated. Results indicate that the PEMFC with gradient sinusoidal-wave fins in cathode channel can achieve higher power density and more uniform membrane current density. This is due to that the gas velocity in cathode channel with gradient sinusoidal-wave fins is significantly increased, leading to better oxygen transport and liquid water removal. Furthermore, effects of the geometrical parameters of gradient sinusoidal-wave fins on the electricity generation performance, membrane current density, and mass fraction of oxygen and liquid water of PEMFC are analyzed and discussed. It is found that the optimum waveform depth growth rate and wavelength of the gradient sinusoidal-wave fins is 0.035 and 2.5 mm, respectively. At 0.5 V, the maximum power density of the PEMFC with gradient sinusoidal-wave fins is 5.3 % higher than that of the PEMFC with conventional channel.

Keywords: Proton exchange membrane fuel cell; Normal sinusoidal-wave fins; Gradient sinusoidal-wave fins; Performance enhancement

Graphical Abstract (for review)

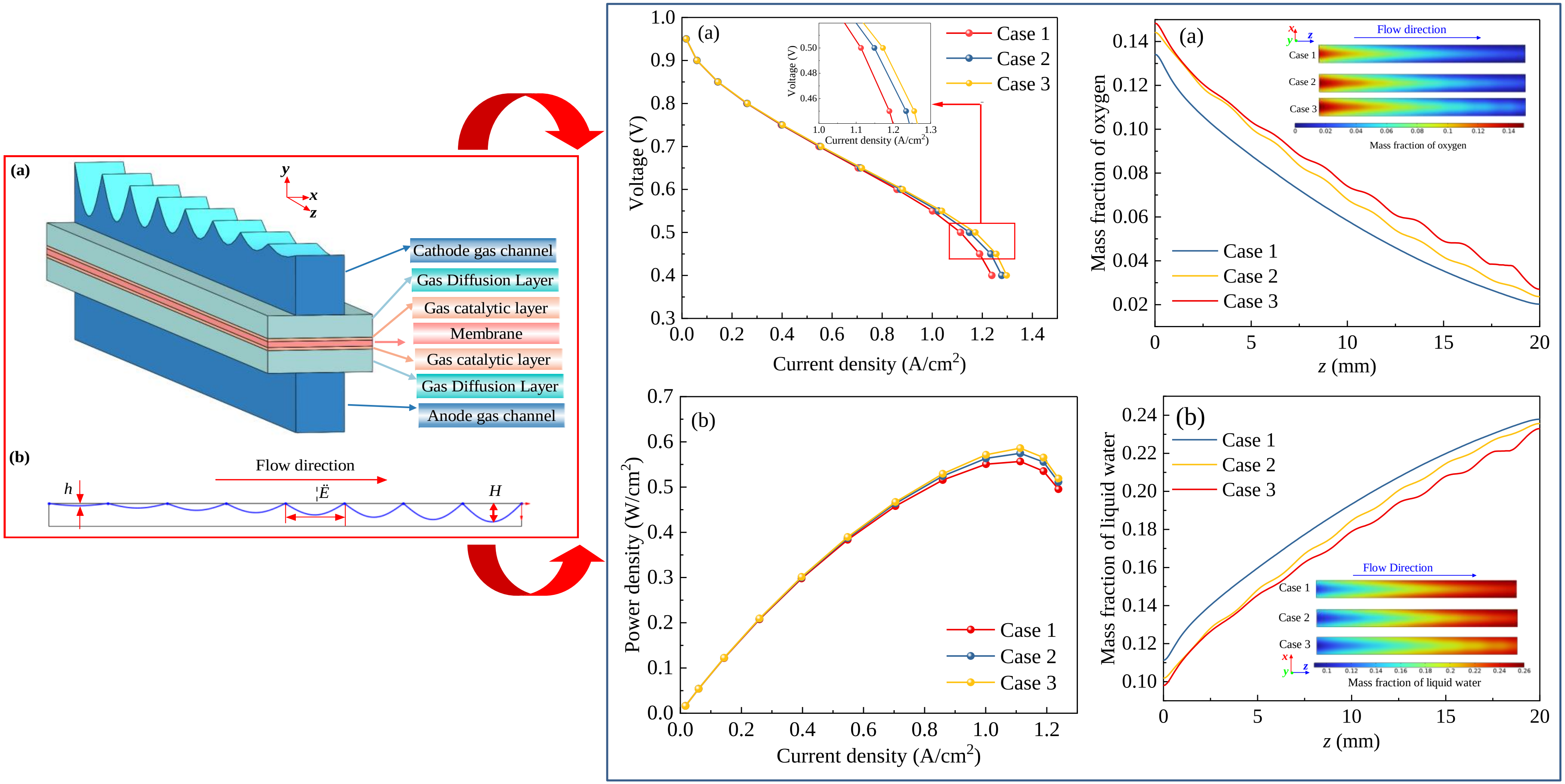

Highlights

1. The gradient sinusoidal-wave fins are used in the cathode channel of PEMFC.
2. PEMFC with gradient sinusoidal-wave fins in cathode channel shows better performance.
3. Effects of geometrical parameters of gradient sinusoidal-wave fins are investigated.
4. Optimum waveform depth growth rate and wavelength is 0.035 and 2.5 mm, respectively.

Nomenclature

c_k molar fraction

D_i mass diffusivity ($m^2\ s^{-1}$)

F constant of Faraday (96485 $C\ mol^{-1}$)

j exchange current density ($A \cdot m^{-3}$)

n_d permeability coefficient

R gas constant (8.314 $J \cdot mol^{-1} \cdot K^{-1}$)

S species source

RH relative humidity

r_w condensation rate

$\vec{u}$ velocity ($m \cdot s^{-1}$)

x mass fraction

Greek letters

ε gas diffusion layer porosity

ρ density

λ stoichiometric ratio

τ membrane water content

α transfer coefficient

μ viscosity

γ specific heat ratio

subscripts

eff effective

f liquid phase

s solid phase

1. Introduction

Recently, with the heavy environmental pollution and increasing energy crisis [1-5], researchers at home and abroad develop lots of interests in proton exchange membrane fuel cells due to their high efficiency, zero emission, short start-up time, low noise, and good adaptability [6-10]. However, the commercialization of PEMFC is still faced with many challenges, such as uneven current density distribution [11-13], low fuel utilization [14-17], and poor membrane stability and durability [18-21].

In order to address the above issue, optimization the flow field of bipolar plate in PEMFC is an effective way, which can facilitate the gas diffusion and enhance the performance and stability of PEMFCs [22-28]. For example, Mohammedi et al. [29] investigated effects of cross-sections of gas flow channel on power density and pressure drop, and the results pointed out that at medium and high current densities, the trapezoidal and inverted trapezoidal top-shaped channels have higher power density, while triangular-shaped channels have higher pressure drop. Vazifeshenas et al. [30] designed a novel compound flow field design including both serpentine and parallel flow fields. The water flooding could be effectively avoided at the high current density. Cai et al. [31] designed a new 3D cathodic flow field including a main pathway, a sub pathway and an excess cathodic flow region, and also proposed a novel evaluation criterion on flow field design. The findings demonstrated that the proposed evaluation criterion was well-suited for assessing the performance of PEMFCs, and the novel cathodic flow field exhibited even more superior performance. Cooper et al. [32] experimentally examined a wide range of critical cathode bipolar plate channel dimensions such as channel/land width and channel depth on cell performance at various conditions. It was found that the channel/land width had most significant effects on both raw power and limiting current density for parallel flow fields, while the stoichiometry was the most important for interdigitated flow fields. Wang et al. [33] designed two novel biophysical flow slabs. Compared with traditional flow channels, it was found that the new biological flow channels could improve the transport capacity of reaction gas and promote the removal of liquid water. Fan et al. [34] proposed and investigated two novel cathode channel designs (multi-plates structure channel and integrated structure channel). Results showed that the two novel channel designs were able to remove more liquid water from PEMFC and effectively avoid from water flooding. The maximum improvement of PEMFC net power densities for the multi-plates structure and integrated structure were 4.7% and 7.5%, respectively. Wang et al. [35] proposed two tapered flow fields with varying height or width. Numerical and experimental results proved that the tapered flow fields with high velocity at the downstream region can significantly enhance water removal in flow channels, avoiding the mass transport limitation and improving the cell performance at high current densities. Additionally, the tapered design could also enhance the under-rib convection between adjacent channels, helping to remove accumulated water in the gas diffusion layer.

Meanwhile, some researchers added obstacles inside the gas channel to improve the performance of PEMFC. Yin et al. [36] installed the inclined baffles in the gas channel, and the results demonstrated that the 45° inclination angle greatly improved the performance of PEMFC. Ebrahimzadeh et al. [37] installed a variety of obstacles in the gas channel, and the results demonstrated that the triangular obstacles can effectively enhance the current density. The current density with a triangular obstacle at 0.6 V was 50% higher than that without the obstacle. Shen et al. [38] improved PEMFC performance by adding rectangular plugs to the channel. It was found that adding plug, especially in the case of high current density, could produce longitudinal eddy current and improve the performance of PEMFC. Tiss et al. [39] proposed partial block inserting into the gas channel. The findings indicated that more reaction gas could enter the gas diffusion layer.

Furthermore, wave and wedge flow channels were paid much attention. Zhang et al. [40] introduced wedge-shaped fins in the cathode channel of a single-channel PEMFC, investigating effects of fin number and GDL porosity. Results indicated that the wedge-shaped fins significantly improved the efficiency of PEMFC. Cai et al. [41] constructed a bio-inspired wave-type channel and demonstrated that the optimal power density was increased by 2.2% when the central amplitude and wave period was 0.305 mm and 3.52, respectively. Chen et al. [42] developed a novel 3D wave flow channel. It was found that the new waveform flow channel could better remove liquid water and promote gas transport. Meanwhile, the current density was enhanced by 23.8% in comparison with the conventional channel at 0.4 V. Kuo et al. [43-44] constructed and investigated a new waveform channel at the operating temperature range of 323 K to 343 K. It was found that the wavy flow channel improved the temperature uniformity and had higher output power density compared the conventional flow channel. Atyabi et al. [45] designed a sinusoidal flow field channel and compared it with the parallel flow field. The results showed that the maximum velocity, pressure drop and power density of the sinusoidal flow field were much higher than that of the parallel flow field.

According to the above studies, the structure of flow channel in bipolar plate has important effects on the performance of PEMFC. In this work, in order to enhance the performance of PEMFC, the gradient sinusoidal-wave fins applied in the cathode channel of PEMFC, and effects of geometrical parameters of the gradient sinusoidal-wave fins on the electricity generation performance, membrane current density, and mass fraction of oxygen and liquid water of PEMFC are investigated. This work will offer us significant reference on designing the cathode channel of PEMFC.

2. Numerical model

2.1. Physical model

The geometrical model of the PEMFC with gradient sinusoidal-wave fins in cathode channel is illustrated in Figure 1(a). Figure 1(b) presents the *xz* cross-section of the cathode channel with gradient sinusoidal-wave fins, and it is displayed that the depth of the gradient sinusoidal-wave fins varies uniformly from the entrance to the exit. For showing the performance enhancement of PEMFC with gradient sinusoidal-wave fins in cathode channel, PEMFCs with conventional cathode channel and sinusoidal-wave fins in cathode channel are selected for comparison. Then, effects of structure parameters of gradient sinusoidal-wave fins (growth rate of waveform depth and wavelength) on the performance of PEMFC are investigated, as illustrated in Figure 2 and Table 1.

Tables 2 and 3 show the geometrical and operation parameters of PEMPC, respectively.

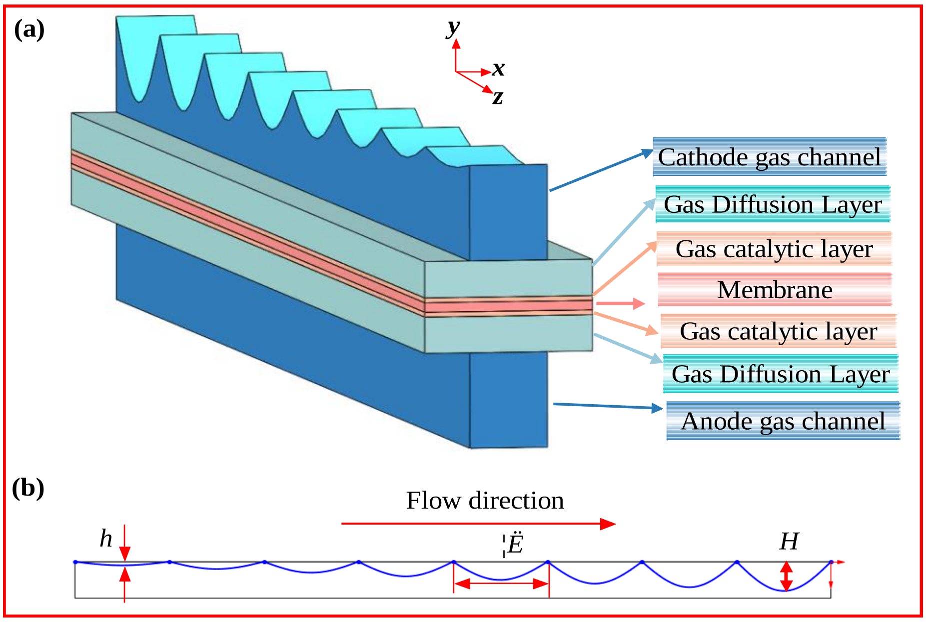

Figure 1 PEMFC model with gradient sinusoidal-wave fins in cathode channel: (a) geometrical model; (b) *xz* cross-section of cathode channel

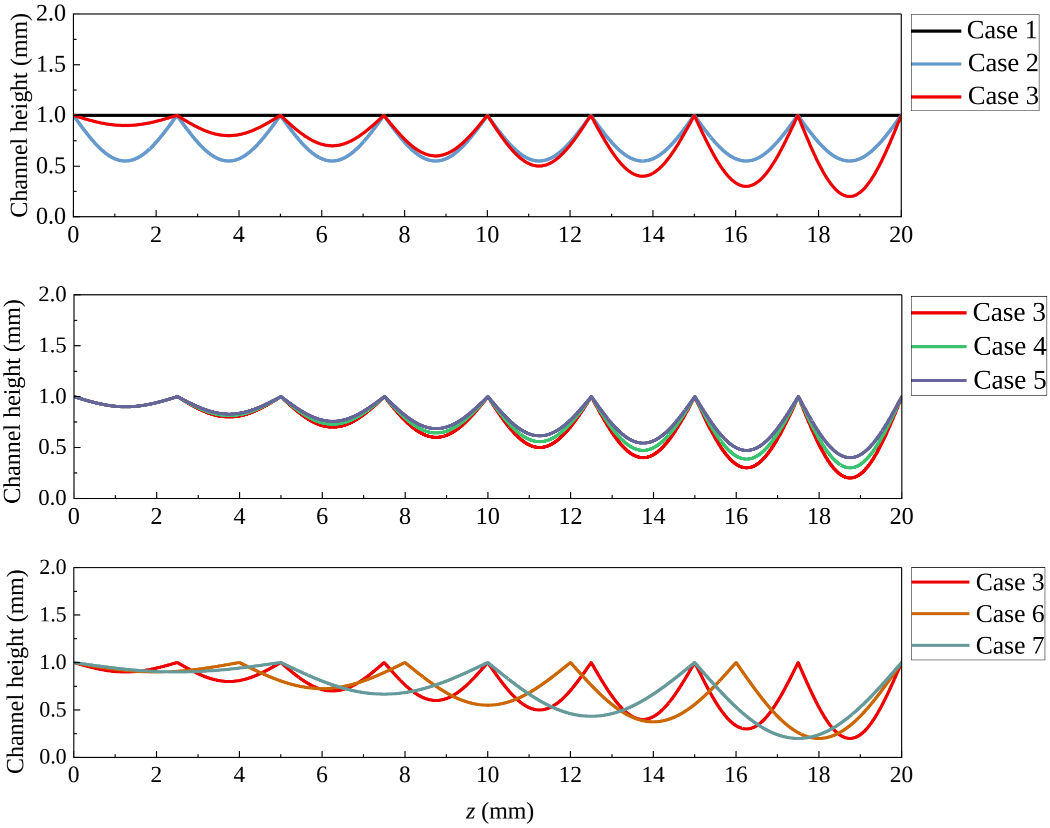

Figure 2 *xz* cross-section of cathode channel with different structure parameters

Table 1 Dimensions of different cathode channels

Case No.	Minimum waveform depth (h)/mm	Maximum waveform depth (H)/mm	Growth rate of waveform depth ($r=(H-h)/20$)	wavelength (λ)/mm
Case 1	-	-	-	-
Case 2	0.45	0.45	0	2.5
Case 3	0.1	0.8	0.035	2.5
Case 4	0.1	0.7	0.03	2.5
Case 5	0.1	0.6	0.025	2.5
Case 6	0.1	0.8	0.035	4
Case 7	0.1	0.8	0.035	5

Table 2 Dimensions of PEMFC with conventional cathode channel

Dimensions	Values (mm)
Channel length	20.0
Membrane thickness	0.1
CL thickness	0.05
Cell width	0.1
Channel width	0.7874
GDL thickness	0.38
Rib width	0.90932
Channel height	1.0

Table 3 Operation parameters

Parameter	Value	Ref
Pressure (Pa)	101325	[42]
Working temperature (T) (K)	343.15	[13]
Reference temperature (T_1) (K)	453.15	[42]
Hydrogen stoichiometric ratio (λ_a)	1.2	[13]
Air stoichiometric ratio (λ_c)	2	[13]
Membrane permeability (m^2)	1.80E-11	[42]
Cathode transfer coefficient	1	[13]
Membrane conductivity ($S\cdot m^{-1}$)	9.825	[42]
H_2 mass fraction	0.96268	[42]
O_2 mass fraction	0.20216	[42]
H_2O mass fraction	0.037319	[42]
Voltage in open circuit (V)	0.95	[42]
Surface-to-volume ratio (1/m)	1.00E+07	[42]
GDL porosity	0.4	[42]
GDL conductivity ($S\cdot m^{-1}$)	222	[42]
GDL permeability (m^2)	2.36E-12	[42]

2.2. Governing equations

Before establishing the 3D multi-phase model of PEMFC [16], the following assumptions are made: (a) PEMFC operates under stable conditions; (b) All porous media are homogeneous; (c) All reaction gases are considered to be incompressible ideal gases; (d) The gas flow can be assumed as laminar due to its low flow rate; (e) Neglecting contact resistance at the contact interface of proton exchange membrane fuel cells. (f) The water transport over the membrane occurs by electroosmotic mechanisms and back diffusion. Simultaneously, the permeability of membrane to the reactants is disregarded.

With the above assumptions, the governing equations for each domain are shown in Table 4.

Table 4 Governing equations

Conservation equations and terms	Mathematical form	Domains
Continuity equation	$\nabla\cdot(\rho u)=0$	GDL, CL, Flow channel
Mass conservation equation	$\nabla\cdot(\varepsilon\rho\vec{u})+\frac{\partial(\varepsilon\rho)}{\partial\tau}=S_{\mathrm{m}}$	GDL, CL, Flow channel
Mass source term	$S_{\mathrm{m}}=-\frac{M_{\mathrm{H_2}}}{2F}R_{\mathrm{a}}-\frac{n_{\mathrm{d}}M_{\mathrm{H_2O}}}{F}R_{\mathrm{a}}$	Anode CL
	$S_{\mathrm{m}}=\frac{M_{\mathrm{H_2O}}}{2F}R_{\mathrm{c}}-\frac{M_{\mathrm{O_2}}}{2F}R_{\mathrm{c}}+\frac{n_{\mathrm{d}}M_{\mathrm{H_2O}}}{F}R_{\mathrm{c}}$	Cathode CL
Conservation of mass equation	$\nabla\cdot(\varepsilon\vec{u}c_{\mathrm{k}})=\nabla\cdot(D_{\mathrm{i,eff}}\nabla c_{\mathrm{k}})+S_{\mathrm{i}}$	GDL, CL, Flow channel
Effective diffusion coefficient	$D_{\mathrm{i,eff}}=\varepsilon^{1.5}(1-s)^{2.5}D_{\mathrm{i}}^{0}(\frac{101325}{p})(\frac{T}{300})^{1.5}$	GDL, CL, Flow channel
Source term of species	$S_{\mathrm{H_2}}=-\frac{M_{\mathrm{H_2}}}{2F}R_{\mathrm{a}}$ $S_{\mathrm{H_2O}}=-\frac{n_{\mathrm{d}}M_{\mathrm{H_2O}}}{F}R_{\mathrm{a}}-r_{\omega}$	Anode CL
	$S_{\mathrm{o_2}}=-\frac{M_{\mathrm{O_2}}}{4F}R_{\mathrm{c}}$ $S_{\mathrm{H_2O}}=\frac{M_{\mathrm{H_2O}}}{2F}R_{\mathrm{c}}+\frac{n_{\mathrm{d}}M_{\mathrm{H_2O}}}{F}R_{\mathrm{a}}-r_{\omega}$	Cathode CL
Conservation of momentum equation	$\frac{1}{\varepsilon^2}\nabla\cdot(\rho\vec{u}\vec{u})=-\nabla p+\frac{1}{\varepsilon}\nabla\cdot(\vec{u}\mu)+S_{\mathrm{u}}$	GDL, CL, Flow channel
Source term of momentum	$S_{\mathrm{u}}=-\frac{\mu}{K}\varepsilon^2\vec{u}$	GDL, CL, Flow channel
Conservation of charge equation	$\nabla\cdot(\delta\cdot\nabla\varphi)+S=0$	In the CL, GDL and

		BP
Conductivity	$\delta = (0.514\tau - 0.326)e^{1268(\frac{1}{303}-\frac{1}{T})}$	Membrane, CL
Source term of the transmitted current	$S = \begin{cases} j & \text{in the CL} \\ 0 & \text{other positions} \end{cases}$	In the CL, GDL and BP
Transfer current density	$j = Ai_0 \left\{ \exp\left[\frac{-\alpha F \Delta V_{act}}{RT}\right] - \exp\left[\frac{(1-\alpha) F \Delta V_{\mathrm{act}}}{RT}\right] \right\}$	CL
Energy equation	$\varepsilon \rho c_{\mathrm{p}} \vec{u} \cdot \nabla T = S_{\mathrm{h}} + \nabla \cdot (k_{\mathrm{eff}} \nabla T)$	All the domains
Thermal conductivity	$k_{\mathrm{eff}} = \varepsilon k_{\mathrm{f}} + (1-\varepsilon) k_{\mathrm{s}}$	All the domains

where φ denotes phase potential, i_0 represents the exchange current density of reference, ΔV_{act} denotes activation over-voltage, k_{f} and k_{s} denote the thermal conductivity of the fluid and solid, respectively.

2.3. Boundary conditions

The velocity at the inlet of the channel is regulated and maintained at a constant under various operation environments [46]:

$$\overrightarrow{u_{\mathrm{in\_c}}} = \frac{\lambda_{\mathrm{c}} \frac{1}{4F} x_{\mathrm{O_2}} RT}{p \cdot A} \tag{1}$$

$$\overrightarrow{u_{\mathrm{in\_a}}} = \frac{\lambda_{\mathrm{a}} \frac{1}{4F} x_{\mathrm{O_2}} RT}{p \cdot A} \tag{2}$$

All exterior walls are presumed to be zero-flux and non-slip with symmetric GDL and CL [47]. The cathode potential is adjusted with an increment of 0.05 V between 0.9 V and 0.4 V in the simulation [48].

2.4. Grid independence study

The software COMSOL 6.0 is employed to solve the above numerical model. In order to make a balance between the computational cost and computational accuracy, the curves about current density vs. voltage under different grid sizes are compared, as depicted in Figure 3. It is observed that the polarization curves are gradually close with the increase of grid number and when the grid number is 17,368 and 20,540, the polarization curves are very similar and differences are hard to be distinguished. In other words, the simulation results remain independent of the grid number when it exceeds 17,368. As a result, the mesh model with a grid number of 17,368 is used in the subsequent simulations.

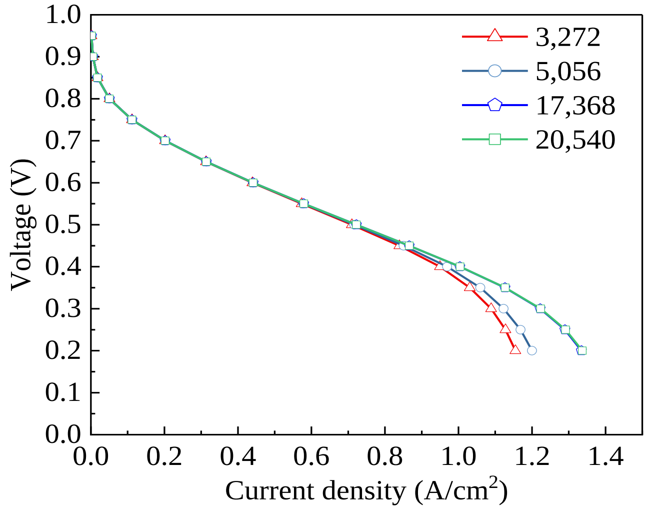

Figure 3 The curves about current density vs. voltage under different grid sizes

2.5. Model validation

Under the same geometric model and experimental conditions, the accuracy of the numerical model is verified by the experimental data obtained from literature [46]. Figure 4 depicts the polarization curves under different pressures by simulation and experiment. The results demonstrate that the polarization curves under simulation are nearly consistent with the experimental results, and the discrepancy falls within the allowable range. This proves that the proposed numerical model is accurate and reliable.

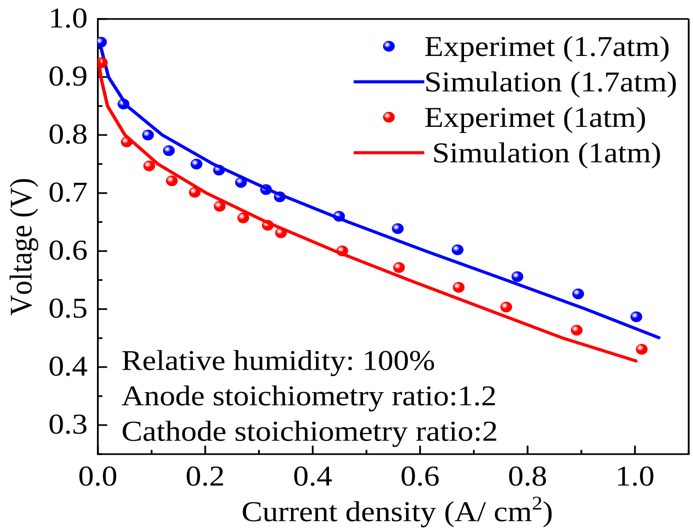

Figure 4 Comparison between polarization curves by simulation and experiment

3. Results and discussion

3.1. Effects of cathode channel structure

Figure 5 shows the gas velocity in the *z* and *y* directions for the conventional channel (Case 1), channel with normal sinusoidal-wave fins (Case 2) and channel with gradient sinusoidal-wave fins (Case 3), respectively. It can be seen that both in the *y*-direction and *z*-direction, the gas velocity in Case 3 is the highest, while that in Case 1 is the lowest. This is also reflected by the following Table 5. It can be clearly seen that the maximum gas velocity at the *y*-direction in the channel with gradient sinusoidal-wave fins arrives at 0.55 m/s. However, the maximum gas velocity at the *y*-direction in the conventional channel is close to zero, meaning that the gas can only enter the gas diffusion layer by diffusion. The increment of the velocity of reaction gas can carry away more liquid water and achieve good liquid water removal efficiency. Thus, the channel with gradient sinusoidal-wave fins is more favorable for the gas transport and improving the performance of the PEMFC compared with the conventional channel and channel with normal sinusoidal-wave fins.

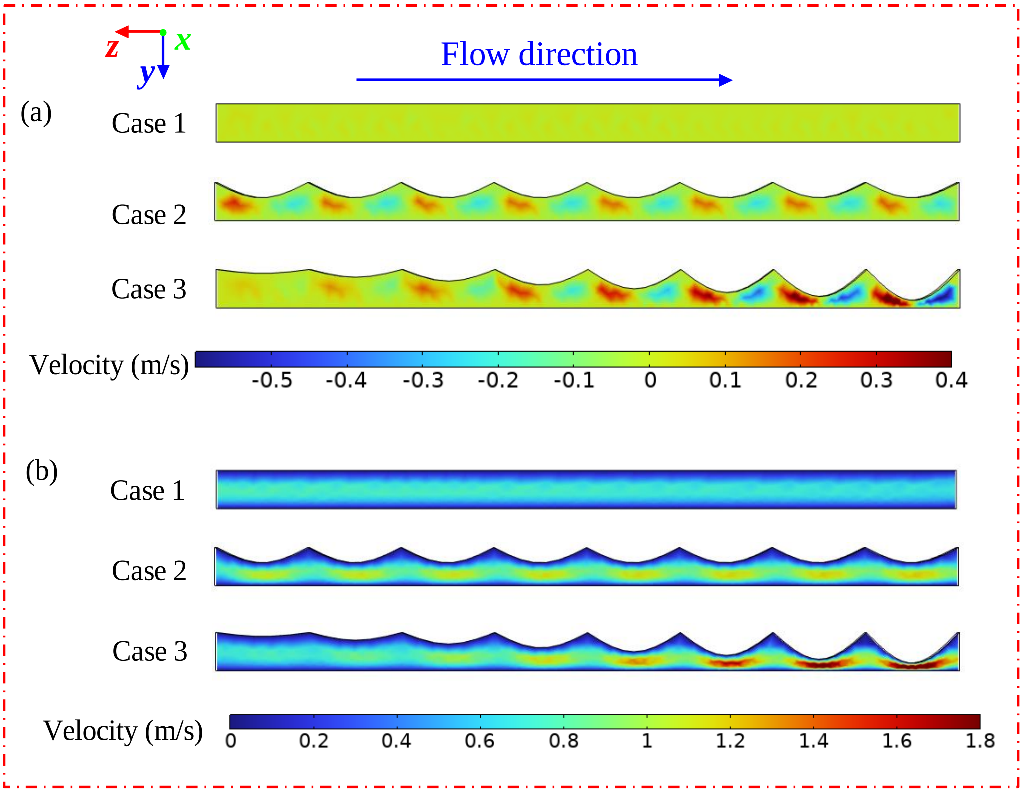

Figure 5 Effects of cathode channel structure on the velocity field of cathode channel at 0.5 V: (a) *y*-direction; (b) *z*-direction

Table 5 Maximum gas velocity at *y*-direction and *z*-direction under different cathode channels

Cathode channel	Maximum gas velocity at *y*-direction (m/s)	Maximum gas velocity at *z*-direction (m/s)
Conventional channel (Case 1)	0.026	0.8
Channel with sinusoidal-wave fins (Case 2)	0.26	1.2
Channel with gradient sinusoidal-wave fins (Case 3)	0.55	2.86

Figure 6 show the polarization curves and power density curves of PEMFC with conventional channel (Case 1), channel with sinusoidal-wave fins (Case 2) and channel with gradient sinusoidal-wave fins (Case 3), respectively. It can be seen in Figure 6 that there is nearly no difference among the polarization curves of PEMFCs with different cathode channels at the range of low current density. However, at the range of high current, the voltage and power density of PEMFC with gradient sinusoidal-wave fins in cathode channel (Case 3) is significantly higher than that with sinusoidal-wave fins in cathode channel and the conventional channel. Moreover, the maximum power density of PEMFC with gradient sinusoidal-wave fins in cathode channel is 5.3% higher than that with conventional channel and 3.2% higher than that with sinusoidal-wave fins in cathode channel at 0.5 V, respectively.

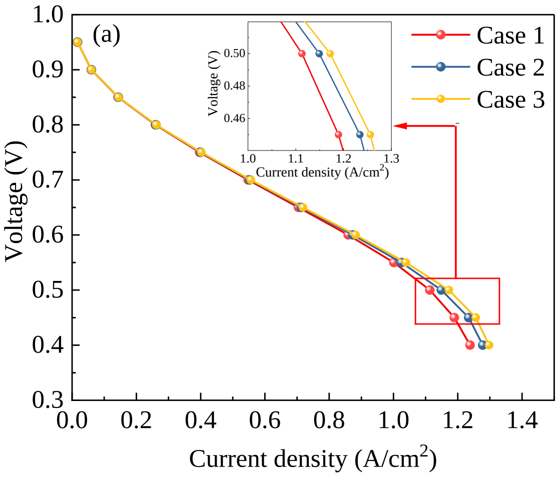

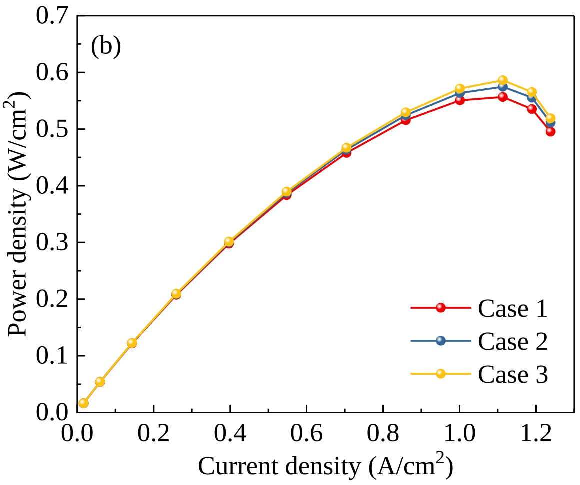

Figure 6 Effects of cathode channel structure on the electricity generation performance of PEMFC: (a) polarization curve; (b) power density curve

The uniformity of the membrane current density distribution greatly affects the output voltage of PEMFC. The more uniform the distribution of membrane current density, the better the performance of the cell. Figure 7 shows the distribution of membrane current density in the PEMFC at 0.5 V for the conventional channel (Case 1), the channel with sinusoidal-wave fins (Case 2) and the channel with gradient sinusoidal-wave fins (Case 3). It is clear that for all the three channels, the current density is gradually reduced from the inlet to the outlet due to the higher concentration of reactants at the inlet. However, the range of membrane current density for the three channels is different, as displayed in Table 6. It is evident that the maximum current densities in the three channels are very close, while the minimum current density in the channel with gradient sinusoidal-wave fins (Case 3) is significantly higher than that of the other two channels. Therefore, the channel with gradient sinusoidal-wave fins has a more uniform membrane current density distribution compared with the channel with sinusoidal-wave fins and the conventional channel.

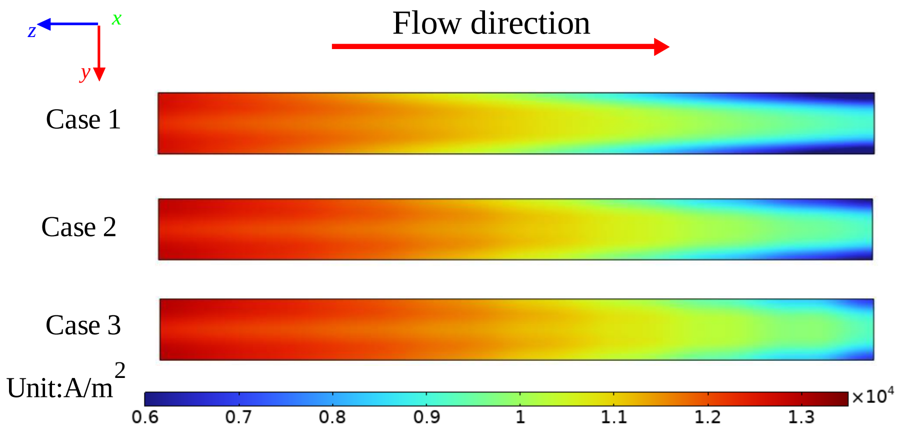

Figure 7 Effects of cathode channel structure on the distribution of membrane current density

Table 6 Maximum and minimum membrane current density under different cathode channels

Cathode channel	Maximum membrane current density (A/m^2)	Minimum membrane current density (A/m^2)
Conventional channel (Case 1)	13219.5	6228.5
Channel with sinusoidal-wave fins (Case 2)	13419.9	7037.3
Channel with gradient sinusoidal-wave fins (Case 3)	13514.9	7814.8

Figure 8(a) presents the mass fraction of oxygen at the centerline of cathode GDL-CL interface for different cathode channels at 0.5 V. It is evident that the mass fraction of oxygen gradually decreases from the entrance to exit, owing to the consumption of oxygen in the electrochemical reaction. In addition, it can be observed that the mass fraction of oxygen in the channel with gradient sinusoidal-wave fins is the highest, followed by the channel with sinusoidal-wave fins and the conventional channel. The results show that the channel with gradient sinusoidal-wave fins facilitates the oxygen transport and improves the oxygen utilization rate compared to the conventional channel.

The accumulation of liquid water will lead to channel blockage, preventing gas from reaching the catalytic layer and causing the increased concentration polarization. Furthermore, it seriously affects the electrochemical reaction inside the PEMFC and further reduces the power density. Figure 8(b) illustrates the mass fraction of liquid water at the centerline of cathode GDL-CL interface for different cathode channels at 0.5 V. It can be observed that the mass faction of liquid water gradually increases from inlet to outlet as oxygen is consumed. It is also found that the liquid water in the conventional channel (Case 1) is the highest, followed by channel with sinusoidal-wave fins (Case 2) and channel with gradient sinusoidal-wave fins (Case 3). Therefore, it can be concluded that the channel with gradient sinusoidal-wave fins is better than the channel with sinusoidal fins and the conventional channel in terms of the ability of the liquid water removal.

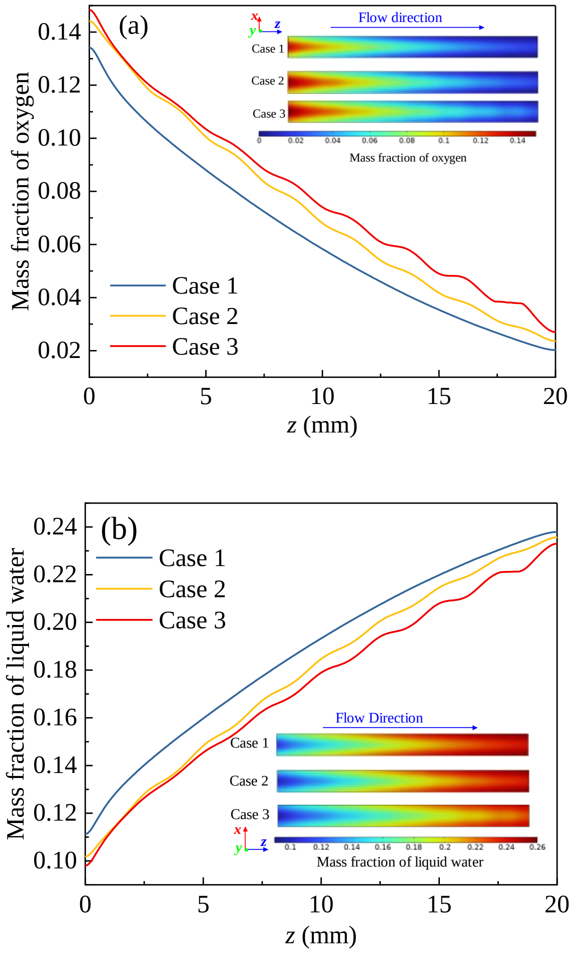

Figure 8 Effects of cathode channel structure on the mass fraction of oxygen and liquid water in the cathode channel at 0.5 V: (a) oxygen; (b) liquid water

3.2. Effects of growth rate of waveform depth

Figure 9 depicts effects of growth rate of waveform depth on the polarization curves and power density curves of the PEMFC with gradient sinusoidal-wave fins in cathode channel. It is evident that the PEMFC with gradient sinusoidal-wave fins in cathode channel achieves the maximum power density at 0.5 V whatever the growth rate of waveform depth is. However, it is still can be observed that the maximum power density is increased with the increment of growth rate of waveform depth.

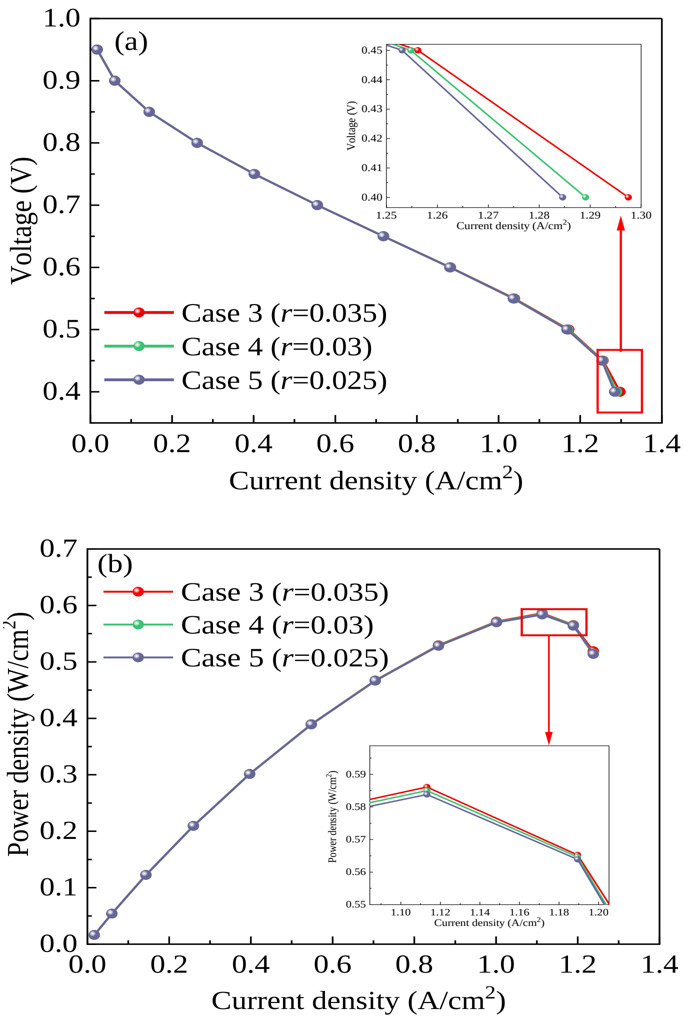

Figure 9 Effect of growth rate of waveform depth on the electricity generation performance of the PEMFC with gradient sinusoidal-wave fins in cathode channel: (a) polarization curve; (b) power density curve

Figure 10 illustrates effects of growth rate of waveform depth on the distribution of membrane current density of PEMFC with gradient sinusoidal-wave fins in cathode channel. It can be seen that with the increment of the growth rate of waveform depth, the membrane current density becomes more uniform, which also can be suggested by Table 7. It is shown that the maximum membrane current density under different growth rates of waveform depth is nearly the same, while the minimum membrane current density is decreased with the reduction of the growth rate of waveform depth. Specifically, when the growth rate of waveform depth is 0.035, 0.03 and 0.025, respectively, the minimum membrane current density arrives at 7814.8 A/m^2, 7750.8 A/m^2 and 7728.5 A/m^2, respectively.

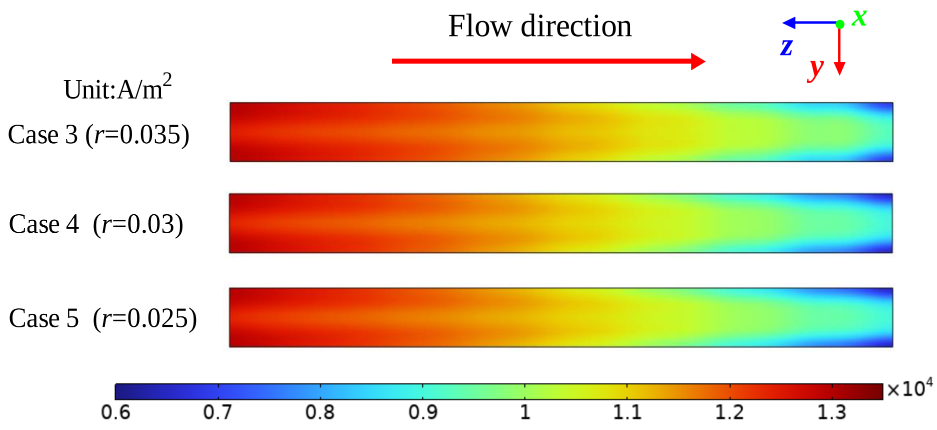

Figure 10 Effects of growth rate of waveform depth on the distribution of membrane current density of PEMFC with gradient sinusoidal-wave fins in cathode channel

Table 7 Maximum and minimum membrane current density under different growth rates of waveform depth

Growth rate of waveform depth	Maximum membrane current density (A/m^2)	Minimum membrane current density (A/m^2)
Case 3 (r=0.035)	13514.9	7814.8
Case 4 (r=0.03)	13515.7	7750.8
Case 5 (r=0.025)	13515.5	7728.5

Figure 11(a) shows effects of growth rate of waveform depth on the mass fraction of oxygen at the centerline of GDL-CL interface of the PEMFC with gradient sinusoidal-wave fins in cathode channel at 0.5 V. It can be seen that in the first half part of the channel, there is almost no difference in the mass faction of oxygen with the reduction of growth rate of waveform depth, but in the last half part of the channel, the mass faction of oxygen is slightly increased with the increment of growth rate of waveform depth. The results show that for the channel with gradient sinusoidal-wave fins, a large growth rate of waveform depth is desired for better oxygen transport and utilization.

Figure 11(b) suggests effects of growth rate of waveform depth on the mass fraction of liquid water at the centerline of GDL-CL interface of the PEMFC with gradient sinusoidal-wave fins in cathode channel at 0.5 V. It is observed that in the first half part of the channel, there is almost no difference in the mass faction of liquid water with the increment of growth rate of waveform depth, but in the last half part of the channel, the mass faction of liquid water is slightly decreased with the increment of growth rate of waveform depth. The results show that for the channel with gradient sinusoidal-wave fins, a large growth rate of waveform depth is desired for better water removal.

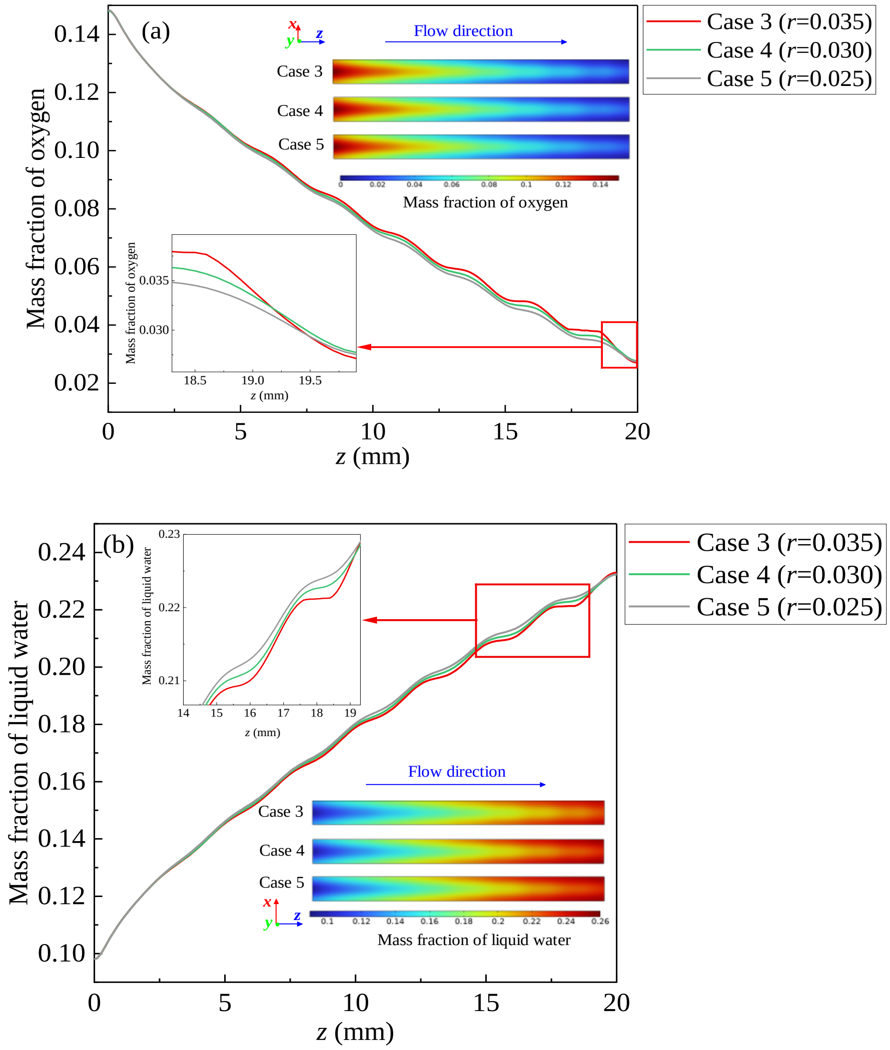

Figure 11 Effects of growth rate of waveform depth on the mass fraction of oxygen and liquid water in the cathode channel at 0.5 V: (a) oxygen; (b) liquid water

3.3. Effects of wavelength

Figures 12 show effects of wavelength on the polarization curves and power density curves of PEMFC with gradient sinusoidal-wave fins in cathode channel. It is clear that the polarization curves are almost identical in the range of low current density, but in the range of high current density, the power density is slightly increased with the reduction of wavelength.

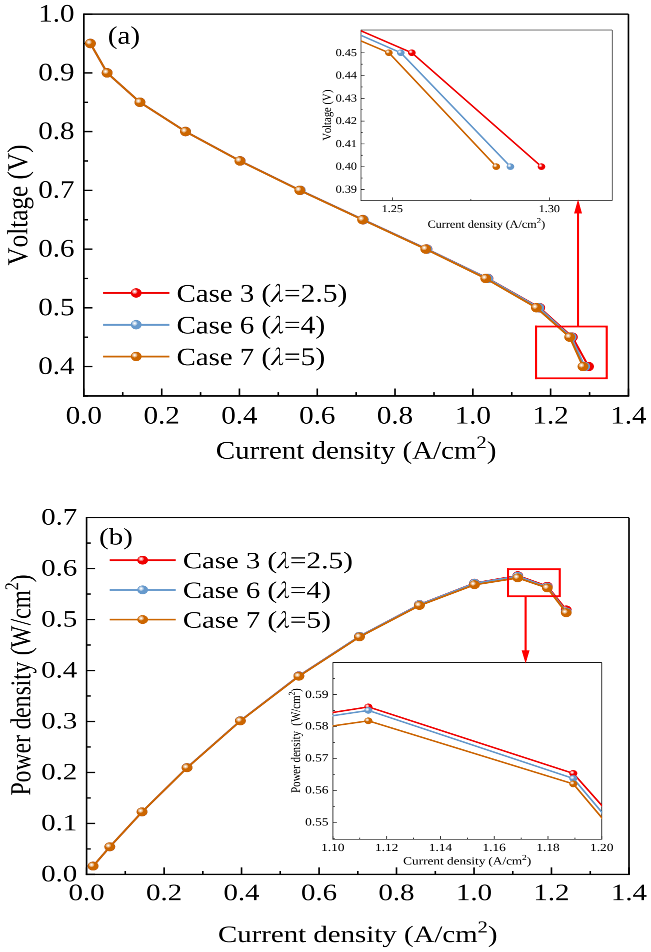

Figure 12 Effects of wavelength on the electricity generation performance of PEMFC with gradient sinusoidal-wave fins in cathode channel: (a) polarization curve; (b) power density curve

Figure 13 shows effects of wavelength on the distribution of membrane current density of PEMFC with gradient sinusoidal-wave fins in cathode channel. It can be observed that with the reduction of wavelength, the membrane current density becomes more uniform, which also can be displayed by Table 8. It is found that when the wavelength is 2.5 mm, 4 mm and 5 mm, respectively, the maximum membrane current density is 13514.9 A/m^2, 13508.5 A/m^2 and 13453.5 A/m^2, respectively, and the minimum membrane current density arrives at 7814.8 A/m^2, 7516.3 A/m^2 and 7067.2 A/m^2, respectively.

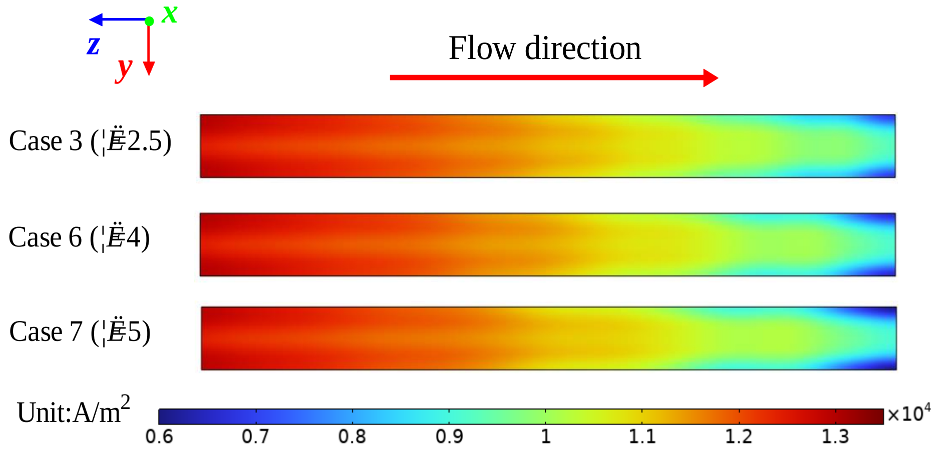

Figure 13 Effects of wavelength on the distribution of membrane current density of PEMFC with gradient sinusoidal-wave fins in cathode channel

Table 8 Maximum and minimum membrane current density under different wavelengths

Wavelength	Maximum membrane current density (A/m^2)	Minimum membrane current density (A/m^2)
Case 3 (λ=2.5)	13514.9	7814.8
Case 6 (λ=4)	13508.5	7516.3
Case 7 (λ=5)	13453.5	7067.2

Figure 14(a) shows effects of wavelength on the mass fraction of oxygen at the centerline of GDL-CL interface of PEMFC with gradient sinusoidal-wave fins in cathode channel. It can be seen that the fluctuation of the variation curve about the mass faction of oxygen is milder with the reduction of wavelength. However, it is still can be found that the mass faction of oxygen is increased with the reduction of wavelength. This means that for the channel with gradient sinusoidal-wave fins, a small wavelength is desired for better oxygen transport and utilization.

Figure 14(b) presents effects of wavelength on the mass fraction of liquid water at the centerline of GDL-CL interface of PEMFC with gradient sinusoidal-wave fins in cathode channel. It can be seen that the fluctuation of the variation curve about the mass faction of liquid water is milder with the reduction of wavelength. However, it is still can be found that the mass faction of liquid water is decreased with the reduction of wavelength. This means that for the channel with gradient sinusoidal-wave fins, a small wavelength is desired for better water removal.

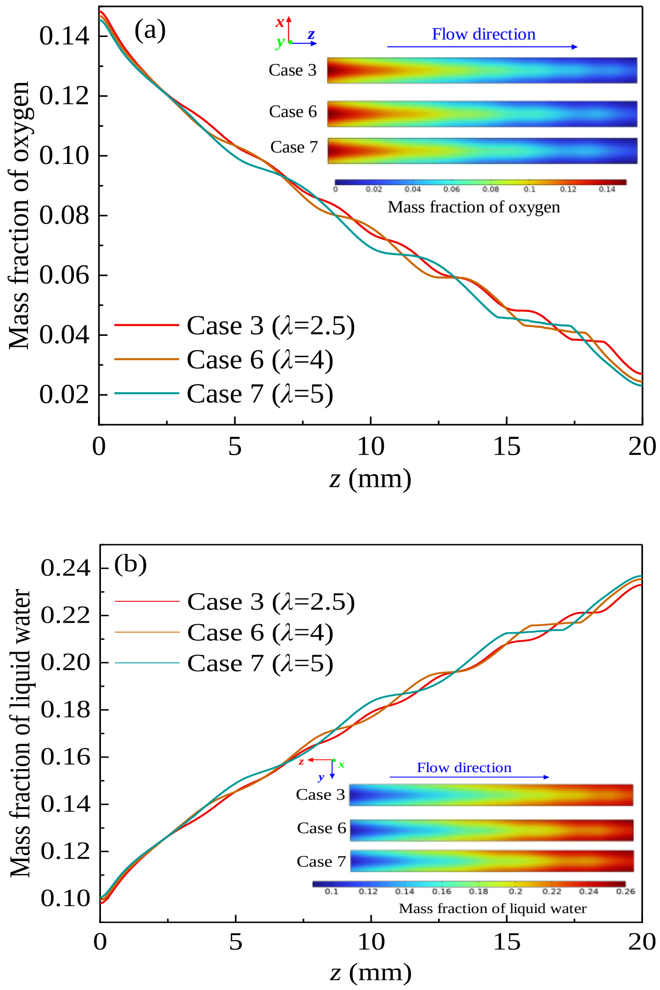

Figure 14 Effects of wavelength on the mass fraction of oxygen and liquid water in the cathode channel at 0.5 V: (a) oxygen; (b) liquid water

4. Conclusions

In this study, a PEMFC with gradient sinusoidal-wave fins in cathode channel is designed. Additionally, effects of the geometrical parameters of gradient sinusoidal-wave fins on the membrane current density, cathode gas velocity, and the mass fraction of oxygen and liquid water are analyzed and discussed. The main conclusions are summarized as follows:

(1) Among the three channels such as conventional channel, channel with sinusoidal-wave fins and channel with gradient sinusoidal-wave fins, the PEMFC with gradient sinusoidal-wave fins in cathode channel can achieve higher power density and more uniform membrane current density. This is due to that the gas velocity in cathode channel with gradient sinusoidal-wave fins is significantly increased, leading to better oxygen transport and liquid water removal.

(2) With the increment of growth rate of waveform depth, the PEMFC with gradient sinusoidal-wave fins in cathode channel can achieve higher power density and more uniform membrane current density, and better oxygen transport and liquid water removal.

(3) As the wavelength decreases, the PEMFC with gradient sinusoidal-wave fins in cathode channel can achieve higher power density and more uniform membrane current density, and better oxygen transport and liquid water removal.

(4) Considering the electricity generation performance, membrane current density, and mass fraction of oxygen and liquid water, the optimum waveform depth growth rate and wavelength of the gradient sinusoidal-wave fins is 0.035 and 2.5 mm, respectively. At 0.5 V, the maximum power density of the PEMFC with gradient sinusoidal-wave fins is 5.3 % higher than that of the PEMFC with conventional channel.

Conflict of Interests

None declared.

Acknowledgments

Dr. Wei Zuo gratefully acknowledges the financial support provided by Natural Science Foundation of Hubei Province (No. 2023AFB029), China Scholarship Council (No. 202308420174), Wuhan University of Science and Technology (No. 1010010) and Wuhan Yellow Crane Talents Program. Dr. Yuhan Huang is a recipient of the ARC Discovery Early Career Research Award (DE220100552).

References

[1] Alharbi AG, Fathy A, Rezk H, Abdelkareem MA, Olabi AG. An efficient war strategy optimization reconfiguration method for improving the PV array generated power. Energy 2023;129129.

[2] Mei B, Barnoon P, Toghraie D, Su C, Nguyen H, Khan A. Energy, exergy, environmental and economic analyzes (4E) and multi-objective optimization of a PEM fuel cell equipped with coolant channels. Renewable and Sustainable Energy Reviews 2022;157:112021.

[3] Barnoon P, Toghraie D, Mehmandoust B, Fazilati M, Eftekhari S. Numerical modeling of species transport and functional characteristics of a proton exchange membrane fuel cell using an agglomerate model with a multi-phase model. Energy Reports 2022; 8:11343-11362.

[4] Wilberforce T, Rezk H, Olabi AG, Epelle EI, Abdelkareem MA. Comparative analysis on parametric estimation of a PEM fuel cell using metaheuristics algorithms. Energy 2023;262:125530.

[5] Mei B, Barnoon P, Toghraie D, Su C, Nguyen H, Khan A. Energy, exergy, environmental and economic analyzes (4E) and multi-objective optimization of a PEM fuel cell equipped with coolant channels. Renewable and Sustainable Energy Reviews 2022; 157:112021.

[6] Kim HR, Seo MH, Ahn JH, Kim TS. Thermodynamic design and analysis of SOFC/PEMFC hybrid systems with cascade effects: A perspective on complete carbon dioxide capture and high efficiency. Energy Reports 2023;9:2335-2347.

[7] Olabi AG, Abdelkarem MA, Jouhara H. Energy Digitalization: Main categories, Applications, Merits and Barriers. Energy 2023;270:126899.

[8] Hu X, Jiang W, Ying X, Eslami M. The application of a new design of bat optimizer for energy efficiency enhancement in PEMFCs based on fractional order theory. Sustainable Energy Technologies and Assessments 2023;55:102904.

[9] Tao Z, Zhang C, Xiong J, Hu H, Ji J, Peng T, Nazir MS. Evolutionary gate recurrent unit coupling convolutional neural network and improved manta ray foraging optimization algorithm for performance degradation prediction of PEMFC. Applied Energy 2023;336:120821.

[10] Lee H, Ryu B, Anh DP, Roh G, Lee S, Kang H. Thermodynamic analysis and assessment of novel ORC-DEC integrated PEMFC system for liquid hydrogen fueled ship application. International Journal of Hydrogen Energy 2023;48(8):3135-3153.

[11] Wu W, Zhai C, Sui Y, Zhang H. A novel distributed energy system using high-temperature proton exchange membrane fuel cell integrated with hybrid-energy heat pump. Energy

Conversion and Management; 2021,235:113990.

[12] Telle JS, Schlüters S, Schönfeldt P, Hanke B, Maydell K, Agert C. The optimized integration of temperature-controlled transports into distributed sector-integrated energy systems. Energy Conversion and Management 2022; 269:116148.

[13] Gabriel RO, Junior ESL, Braga SL, Pradelle F, Serra ET, Vieira CLCS. Technical, economic and environmental analysis of a hybrid CHP system with a 5 kW PEMFC, photovoltaic panels and batteries in the Brazilian scenario. Energy Conversion and Management 2022;269:116042.

[14] Taş M, Elden G. An experimental investigation of the effects of operating conditions on anisotropic electrical conductivity in a PEM fuel cell. Fuel Cells 2020; 20(5):531-539.

[15] Sheng C, Fu J, Li D, Jiang C, Guo Z, Li B, Lei J, Zeng L, Deng Z, Fu X, Li X. Energy management strategy based on health state for a PEMFC/Lithium-ion batteries hybrid power system. Energy Conversion and Management 2022;271:116330.

[16] Shahverdian MH, Sohani A, Sayyaadi H. A 3E water energy nexus based optimum design for a hybrid PV-PEMFC electricity production systems for off-gird applications. Energy Conversion and Management 2022;267:115911.

[17] Chen Z, Zuo W, Zhou K, Li Q, Huang Y, E J. Multi-objective optimization of proton exchange membrane fuel cells by RSM and NSGA-II. Energy Conversion and Management 2023;277:116691.

[18] Shroti N, Daletou MK. The Pt–Co alloying effect on the performance and stability of high temperature PEMFC cathodes. International Journal of Hydrogen Energy 2022;47(36):16235-16248.

[19] Shen X, Liang X, Xu Y, Yu W, Li Q, Ge X, Wu L, Xu T. In-situ growth of PPy/MnOx radical quenching layer for durability enhancement of proton exchange membrane in PEMFCs. Journal of Membrane Science 2023;121556.

[20] Neofytidis C, Paloukis F, Athanasopoulos N, Neophytides SG, Daletou MK. Efficient high temperature PEMFC metallic stack with innovative two-phase liquid cooling. Energy

Conversion and Management 2023;283:116944.

[21]Shang K, Han C, Jiang T, Chen Z. Numerical study of PEMFC heat and mass transfer characteristics based on roughness interface thermal resistance model. International Journal of Hydrogen Energy 2023;48(20):7460-7475.

[22]Guan D, Pan B, Chen Z, Li J, Shen H, Pang H. Quantitative modeling and bio-inspired optimization the clamping load on the bipolar plate in PEMFC. Energy 2023;263:125951.

[23]Park D, Ham S, Sohn YJ, Choi YY, Kim M. Mass transfer characteristics according to flow field and gas diffusion layer of a PEMFC metallic bipolar plate for stationary applications. International Journal of Hydrogen Energy 2023;48(1):304-317.

[24]Ghasabehi M, Jabbary A, Shams M. Cathode side transport phenomena investigation and Multi-Objective optimization of a tapered parallel flow field PEMFC. Energy Conversion and Management 2022;265:115761.

[25]Wang Y, Sun ZY, Yang L. Enhancement effects of the obstacle arrangement and gradient height distribution in serpentine flow-field on the performances of a PEMFC. Energy Conversion and Management 2022;252:115077.

[26]Huang W, Jian Q, Feng S, Huang Z. A hybrid optimization strategy of electrical efficiency about cooling PEMFC combined with ultra-thin vapor chambers. Energy Conversion and Management 2022;254:115301.

[27]Fan L, Xing L, Tu Z, Chan SH. A breakthrough hydrogen and oxygen utilization in a H2-O2 PEMFC stack with dead-ended anode and cathode. Energy Conversion and Management 2021;243:114404.

[28]Wilberforce T, Olabi AG, Pritchard D, Abdelkareem MA, Sayed ET. Development of proton exchange membrane fuel cell flow plate geometry design. Energy 2023; 283: 128854.

[29]Mohammedi A, Sahli Y, Moussa HB. 3D investigation of the channel cross-section configuration effect on the power delivered by PEMFCs with straight channels. Fuel 2020;263:116713.

[30] Vazifeshenas Y, Sedighi K, Shakeri M. Numerical investigation of a novel compound flow-field for PEMFC performance improvement. International Journal of Hydrogen Energy 2015;40(43):15032-15039.

[31] Cai Y, Fang Z, Chen B, Yang T, Tu Z. Numerical study on a novel 3D cathode flow field and evaluation criteria for the PEM fuel cell design. Energy 2018; 161: 28-37.

[32] Cooper NJ, Smith T, Santamaria AD, Park JW. Experimental optimization of parallel and interdigitated PEMFC flow-field channel geometry. International Journal of Hydrogen Energy 2016;41(2):1213-1223.

[33] Wang CT, Hu YC, Zheng PL. Novel biometric flow slab design for improvement of PEMFC performance. Applied Energy 2010;87(4):1366-1375.

[34] Fan L, Niu Z, Zhang G, Jiao K. Optimization design of the cathode flow channel for proton exchange membrane fuel cells. Energy Conversion and Management 2018;171:1813-1821.

[35] Wang C, Zhang Q, Lu J, Shen S, Yan X, Zhu F. Effect of height/width-tapered flow fields on the cell performance of polymer electrolyte membrane fuel cells. International Journal of Hydrogen Energy 2017;42(36):23107-23117.

[36] Yin Y, Wang XF, Zhang JF, Xiang SG, Qin YZ. Influence of sloping baffle plates on the mass transport and performance of PEMFC. International Journal of Energy Research 2019;43(7):2643-2655.

[37] Ebrahimzadeh AA, Khazaee I, Fasihfar A. Experimental and numerical investigation of obstacle effect on the performance of PEM fuel cell. International Journal of Heat and Mass Transfer 2019;141:891-904.

[38] Shen J, Zeng L, Liu Z, Liu W. Performance investigation of PEMFC with rectangle blockages in Gas Channel based on field synergy principle. Heat and Mass Transfer 2019;55:811-822.

[39] Tiss F, Chouikh R, Guizani A. A numerical investigation of reactant transport in a PEM fuel cell with partially blocked gas channels. Energy conversion and management 2014;80:32-38.

[40] Zhang S, Qu Z, Xu H, Talkhoncheh FK, Liu S, Gao Q. A numerical study on the performance

of PEMFC with wedge-shaped fins in the cathode channel. International Journal of Hydrogen Energy 2021;46(54):27700-27708.

[41] Cai G, Liang Y, Liu Z, Liu W. Design and optimization of bio-inspired wave-like channel for a PEM fuel cell applying genetic algorithm. Energy 2020;192:116670.

[42] Chen X, Yu Z, Yang C, Chen Y, Jin C, Ding YJ, Li WB, Wan ZM. Performance investigation on a novel 3D wave flow channel design for PEMFC. International Journal of Hydrogen Energy 2021;46(19):11127-11139.

[43] Kuo JK, Chen C. The effects of buoyancy on the performance of a PEM fuel cell with a wave-like gas flow channel design by numerical investigation. International Journal of Heat and Mass Transfer 2007;50(21-22):4166-4179.

[44] Kuo JK, Yen TH. Three-dimensional numerical analysis of PEM fuel cells with straight and wave-like gas flow fields channels. Journal of Power Sources 2008;177(1):96-103.

[45] Atyabi SA, Afshari E. A numerical multiphase CFD simulation for PEMFC with parallel sinusoidal fields. Journal of Thermal Analysis and Calorimetry 2019;135:1823-1833.

[46] Ubong EU, Shi Z, Wang X. Three-dimensional modeling and experimental study of a high temperature PBI-based PEM fuel cell. Journal of The Electrochemical Society 2009;156(10):B1276.

[47] Chen X, Li W, Gong G, Wan ZM, Tu ZK. Parametric analysis and optimization of PEMFC system for maximum power and efficiency using MOEA/D. Applied Thermal Engineering 2017;121:400-409.

[48] Li H, Xu B, Lu G, Du CH, Huang N. Multi-objective optimization of PEM fuel cell by coupled significant variables recognition, surrogate models and a multi-objective genetic algorithm. Energy Conversion and Management 2021;236:114063.